Universal Relationship between Magnetization and Changes in the Local Structure of $La_{1-x}Ca_xMnO_3$: Evidence for Magnetic Dimers

L. Downward,[1] F. Bridges,[1] S. Bushart,[1] J. J. Neumeier,[2] N. Dilley,[3] and L. Zhou[4]

[1]*Physics Department, University of California, Santa Cruz, California 95064, USA*
[2]*Department of Physics, Montana State University, Bozeman, Montana 59717, USA*
[3]*Quantum Design Inc., 11578 Sorrento Valley Road, San Diego, California 92121-1311, USA*
[4]*Stanford Synchrotron Radiation Laboratory, Stanford Linear Accelerator Center, Menlo Park, California 94025, USA*

(Received 17 May 2004; revised manuscript received 18 November 2004; published 2 September 2005)

We present extensive x-ray absorption fine structure measurements on $La_{1-x}Ca_xMnO_3$ as a function of the B field (to 11 T) and Ca concentration, x (21%–45%). These results reveal local structure changes (associated with polaron formation) that depend only on the magnetization for a given sample, irrespective of whether the magnetization is achieved through a decrease in temperature or an applied magnetic field. Furthermore, the relationship between local structure and magnetization depends on the hole doping. A model is proposed in which a filamentary magnetization initially develops via the aggregation of pairs of Mn atoms involving a hole and an electron site. These pairs have little distortion and it is likely that they form at temperature T^* above T_c.

DOI: 10.1103/PhysRevLett.95.106401 PACS numbers: 71.38.−k, 61.10.Ht, 71.27.+a, 75.47.Lx

In recent years, the interest in manganites has grown significantly. They belong to a broader class of materials where charge-spin-lattice interactions play a crucial role in the observed properties. An understanding of these interactions in the manganites may provide insight into other strongly correlated electron systems, such as the high-T_c superconductors.

The quasicubic manganites ($La_{1-x}Ca_xMnO_3$) exhibit colossal magnetoresistance for Ca concentrations $x \sim 0.2$–0.5. Within this range, there are significant structural changes as a function of temperature observed at the local atomic level [changes in the Mn-O pair distribution function (PDF)] and macroscopically (magnetostriction). The local distortions are associated with polarons and decrease rapidly through and below the ferromagnetic transition as observed using x-ray-absorption fine structure spectroscopy (XAFS) [1–4] and neutron PDF analysis [5] at $B = 0$ T. A tiny B-induced effect at 1 T has also been observed [6], but the effect is too small at 1 T to explore the field dependence.

Many have argued for phase separation [7] or two fluid [2,8] models formed of conducting, ferromagnetic clusters/regions interspersed with poorly conducting regions. Recently, Ramakrishnan *et al.* [9] have proposed a two band model of *coexisting* localized Jahn-Teller (JT) polaron and broadband states. The idea of phase separation in these materials is generally accepted; however, the microscopic details of how nanoscale clusters develop into a fully magnetized state is still poorly understood. Here we propose a mechanism in which Mn pairs form filamentary clusters which are interspersed with Jahn-Teller-distorted, nonmagnetic regions. This is consistent with Kumar *et al* [10], who have shown evidence for small clusters above T_c, where the magnetic susceptibility fits a Curie-Weiss law with a Curie constant nearly twice the expected value, suggesting Mn dimers. In addition, recent neutron scattering data [11] show a glasslike phase with short range order above T_c, which is also consistent with the Mn-dimer model presented here.

Previously, we have shown for a few samples [2,12] that the decrease in average local distortion, $\Delta(\sigma^2)$, as T is decreased below T_c, is a simple function of the sample magnetization, M. Here σ is the width of the Mn-O PDF obtained from extended XAFS (EXAFS), and $\Delta(\sigma^2)$ is the T- or B-induced change in σ^2. By extending those measurements to high fields (9–11 T) for some samples, and to a range of Ca concentrations, $0.21 \leq x \leq 0.45$, we find that the plots of $\Delta(\sigma^2)$ versus M (each normalized to their value at low T) depend primarily on hole concentration.

We find three important results *for each sample*: (i) little distortion is removed until the fraction of magnetized sites (M/M_0) reaches $\sim 2y$, where y is the hole concentration (ii) above $\sim 2y$, distortions are removed more rapidly as the sample becomes fully magnetized, and (iii) the point of change between these two behaviors occurs at $M/M_0 \sim 2y$. In addition, for the samples measured in an applied B field, the above three results hold regardless of field, indicating that the change in local structure depends only on magnetization.

Transmission XAFS Mn K-edge data were collected on powdered samples at the Stanford Synchrotron Radiation Laboratory on beam lines 7–2, 10–2, and 6–2, using a Si(111) monochromator. The sample preparation has been described earlier [2] and accurate hole concentrations, y, were determined by iodometric titration with an uncertainty of ± 0.005. For the XAFS samples, the pressed pellets were reground, passed through a 400-mesh sieve, and then brushed onto scotch tape which preferentially holds the smaller grains (≤ 5 μm) in a thin layer. Layers of tape were stacked to obtain a Mn K-edge absorption step height ($\mu_{\mathrm{Mn}}t$) ~ 0.5 for each sample. Generally, four scans were collected at each T (and B field) for each sample. For

the B-field measurements, the field was aligned parallel to the tape layers such that the demagnetization factor is negligible. The magnetization data were collected on long rods with the B field parallel to the axis; the demagnetization factor for this orientation is also negligible. The upper panel of Fig. 1 displays the magnetization at various magnetic fields for the 30% Ca sample; an applied B field broadens the curve and shifts it to higher temperature.

In EXAFS analysis, the absorption μ_p from other atoms (preedge absorption) is removed first, then a sum of splines is used to obtain the background absorption μ_0 above the edge [13,14]. Next the XAFS function, χ, is obtained as a function of photoelectron wave vector from $\chi(k) = \mu/\mu_0 - 1$ (where $k = \sqrt{2m_e(E - E_0)/\hbar^2}$). See Fig. 2 of Ref. [2] for an example of the data quality. The $k\chi(k)$ data are then Fourier transformed (FT) to r space. An expanded view of the first Mn-O r-space peak for $La_{0.7}Ca_{0.3}MnO_3$ for T near T_c at several fields is plotted in Fig. 1, bottom. As B increases, the amplitude of the Mn-O peak increases; thus the average value of σ must decrease, as observed (see Fig. 2, bottom). In contrast, for $T \ll T_c$ or $T \gg T_c$, no significant B-field induced change in σ is observed. Similar B-field induced changes were observed for the 21% sample for T near T_c. Changes in the Mn-O peak as a function of temperature also correlate with T_c for all samples.

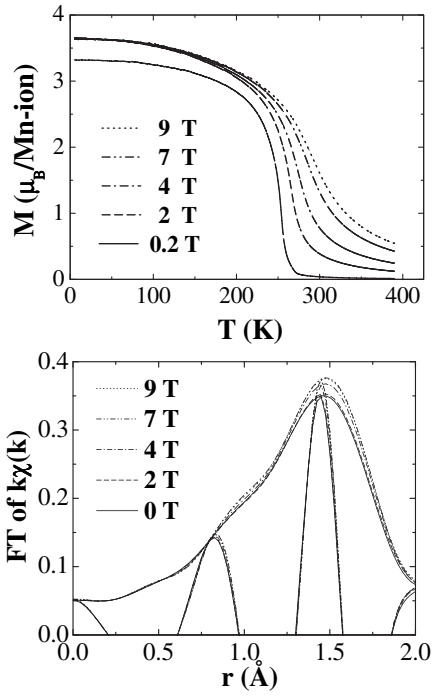

FIG. 1. Top: Magnetization versus T for $La_{0.7}Ca_{0.3}MnO_3$. Bottom: The r-space peak for the Mn-O bond ($La_{0.7}Ca_{0.3}MnO_3$) near $T_c \sim 260$ K. The fast oscillation is the real part of the transform (FT_R) while the envelope is $\pm\sqrt{FT_R^2 + FT_I^2}$, where FT_I is the imaginary part. The FT range is 3.5–11.5 Å, with 0.3 $Å^{-1}$ Gaussian broadening.

The r-space data were fit [14] to similarly transformed standard functions, calculated using the FEFF6 code [15]. We used E_0 and S_0^2 determined in earlier studies [2], constrained the number of neighbors to 6, and fit the first Mn-O peak using an average bond length and a single broadening parameter σ [16]. This method of fitting provides a single-parameter-measure of the local disorder for comparisons with M. For each temperature, separate fits were made to each of four traces and the average value of σ calculated; the rms fluctuation about the average, gives the relative errors, which are comparable to the symbol size in most cases (See Fig. 2). The absolute error for σ^2 depends on the errors in S_0^2 and in the FEFF calculation (both systematic errors), and may be of order 10%–15%. This error primarily changes the static component of σ^2, and shifts the σ^2 versus T plot vertically.

$\sigma^2(T/T_c)$ for the Mn-O peak is plotted in Fig. 2 for 30% and 45% Ca. For the 30% sample, the curves shift to higher T and broaden as B increases, as is also observed in the magnetization measurements (see Fig. 1, top).

The contributions to $\sigma^2(T)$ add up in quadrature when different broadening mechanisms are uncorrelated, i.e., $\sigma^2(T) = \sigma^2_{\text{phonons}}(T) + \sigma^2_{\text{static}} + \sigma^2_{\text{polaron}}(T)$, where $\sigma^2_{\text{phonons}}(T)$ is the contribution from thermal phonons, σ^2_{static} arises from temperature independent static distortions, and $\sigma^2_{\text{polaron}}(T)$ is the contribution from the presence of hopping polarons, at 300 K (which we will argue below, are likely hopping ''dimerons''). The latter becomes T

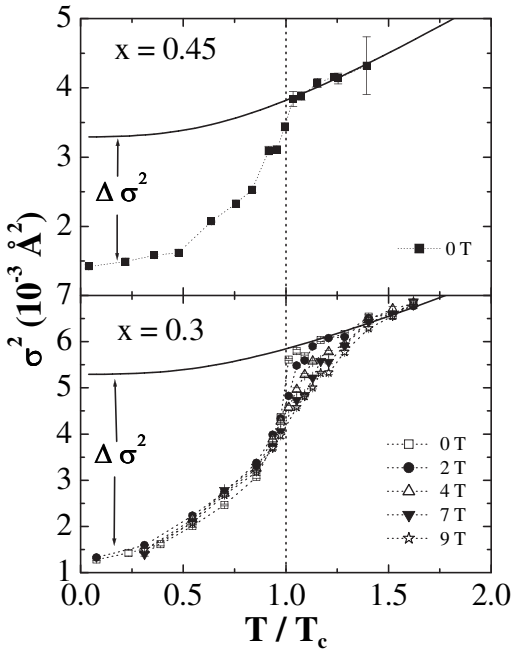

FIG. 2. σ^2 versus T/T_c for the first Mn-O peak of $La_{0.55}Ca_{0.45}MnO_3$ ($T_c \sim 250$ K) and $La_{0.7}Ca_{0.3}MnO_3$ ($T_c \sim 260$ K). The dotted lines are guides to the eye. The solid line is the behavior if no polaron distortions are removed—i.e., σ^2 for $CaMnO_3$ plus a large static distortion. $\Delta(\sigma^2)$ is defined as the difference between this line and the experimental data.

independent when $M \sim 0$—we refer to this as $\sigma^2_{\mathrm{RT-polaron}}$; the remaining weak T dependence just above T_c is nearly identical to that for pure $CaMnO_3$ [2] and arises from the thermal phonon contributions; the solid line in Fig. 2 is the sum of the phonon and RT-polaron distortion. The difference between this line and the data is $\Delta(\sigma^2(T))$ and represents the amount of polaron distortion removed (Fig. 2). Using $\Delta(\sigma^2(T))$ and $M(T)$, we can plot the changes in the local distortions as a function of M. In Fig. 3, we show $\Delta(\sigma^2)$ versus M, with each normalized to their low-T values. The data follow the same linear relationship, within the errors, irrespective of whether the magnetization was obtained by a change in T or B (for $x = 0.3$ and 0.21). Thus, for a given sample, the distortion removed is a nearly universal function of M. An important feature of every plot is the low initial slope; little distortion is removed until the sample is more than 50% magnetized. Then $\Delta(\sigma^2(T))$ increases rapidly with M—i.e., M and $\Delta(\sigma^2)$ are not quite in phase. The breakpoint occurs at $M/M_0 \sim 2y$ for each sample (see Fig. 4) [17], i.e., twice the number of holes. The breakpoint at $\sim 2y$ and the low slope for $M/M_0 < 2y$ suggests that the magnetization develops via pairs of Mn sites—a hole and a (distorted) electron site. We propose that such dimer pairs (which we call a dimeron) form at some temperature T^* [18] above T_c, which likely corresponds to the temperature at which there is a break in the susceptibility plots [10].

In this dimeron model, an electron must be able to rapidly hop back and forth between two sites for the double exchange mechanism to be operative; this is only feasible for an electron-hole pair. For the JT distorted site it costs energy E_{JT} to completely undistort the site; consequently, as long as holes are present, the least amount of energy is required when the magnetization develops in electron-hole pairs. The dimeron quasiparticle will also be mobile; the hole changes electron partners as it moves through the sample.

If we let the distortion per JT site be a constant, α, then the maximum average distortion removed per magnetized Mn site (for decreasing T or increasing B field) is only $\alpha/2$ in the initial stages of magnetization. Once the holes are used up, the distortion removed per Mn site would then increase to α. This is qualitatively close to the behavior of the data shown in Fig. 3; however, the ratio of the slopes is closer to 1:4, instead of 1:2, as would be expected from this simple calculation. However for the dimeron, the electron is partially delocalized and the JT-like distortion will be reduced, although not eliminated. As a result, the ratio of the slopes would be larger than 1:2. For example, if the dimeron contains half the total polaron distortion of an electron-hole pair, then the distortion per site would be $\alpha/4$ and the ratio of slopes would be 1:4.

Another explanation for the large change in slope could be a variation in the size of the polaron distortions (different values of E_{JT}) throughout the system, due to strains and local variations in Ca content. The sites with the smallest distortion would then magnetize first. Since EXAFS gives a measure of the average local distortion over all sites, we cannot easily distinguish between these two possible explanations, unless at higher temperatures the dimerons dissociate to form isolated Mn moments [10] with larger JT polaron distortions. Further experiments are underway to investigate this possibility. Also, as T approaches T_c it is possible that small clusters of dimerons can form: the EXAFS data are not in conflict with such a possibility, they only indicate that equal numbers of electrons and holes (i.e., an integer number of pairs) have aggregated in the magnetic clusters. The EXAFS data, however, are not consistent with a large number of Mn triplets (e.g., two electrons and one hole or two holes and one electron).

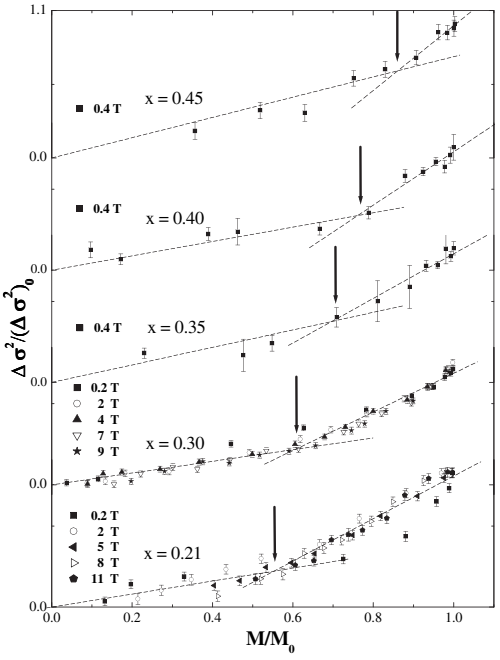

FIG. 3. $\Delta(\sigma^2)$ versus relative magnetization for the five different concentrations. $\Delta(\sigma^2)$ and M have been normalized to their respective values at low T. $\Delta(\sigma^2)$, defined in Fig. 2, is the decrease in σ^2 as T is lowered below T_c that is attributed to the loss of polaronic distortion. Note that the slope of $\Delta(\sigma^2)$ versus M/M_0 changes at roughly $M/M_0 \sim 2y$ (see Fig. 4).

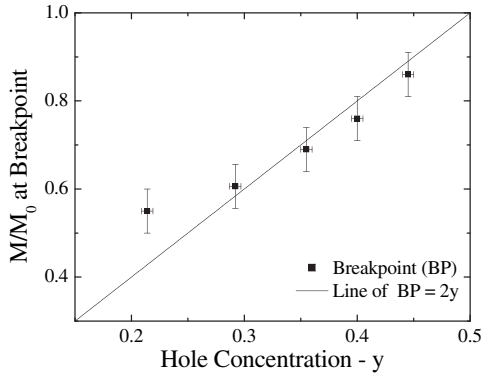

FIG. 4. Breakpoint in Fig. 3 versus hole concentration, y. The breakpoint occurs at $\sim 2y$ for each sample.

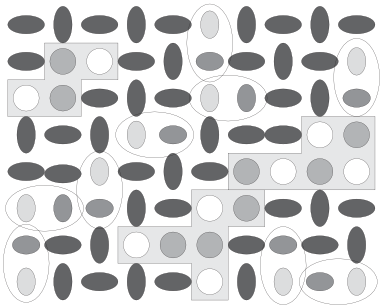

FIG. 5. Model of magnetization process for $T \sim T_c$ (only Mn sites shown). Black ovals—JT-distorted polarons; encircled pairs—dimerons consisting of a partially distorted electron-hole pair; outlined regions—magnetic clusters with magnetized hole sites (open circles) and magnetized electron sites, with JT distortion removed (gray circles).

A "cartoon" of this model for $T \sim T_c$ is depicted in Fig. 5. Pairs of partially distorted holes (small light gray ovals) and partially distorted electron Mn sites (small gray ovals) are encircled at some instant in time, to represent a dimeron; these are continuously hopping as the hole changes electron partners. Several magnetized clusters are also shown; in each cluster, the dimerons become completely undistorted and lose their identity as the electron becomes much more delocalized (initial electron sites represented by gray circles; initial hole sites by open circles) [19]. At low M ($M/M_0 < 2y$), the dimerons in the nonmagnetic regions are continually hopping and will occasionally diffuse close enough to a magnetic cluster that they can join the cluster. Here the quenched disorder from the positions of the Ca constrains how the magnetization develops, because for charge neutrality, the holes cannot be too far away from Ca sites. Consequently, if the magnetic clusters for $M/M_0 < 2y$ are formed from dimeron aggregation, then there will be filaments of the excess JT-distorted electron sites (black ovals) throughout the magnetized regions. Thus, the magnetic cluster development in this regime may be similar to diffusion limited aggregation, with the majority of the magnetic thermal fluctuations occurring in the paramagnetic and boundary regions. It will lead to interpenetrating nanoscale filamentary clusters of magnetic and nonmagnetic regions.

In summary, XAFS data as a function of B and T indicate that the decrease in lattice distortion with increasing M is a nearly universal function for each sample. The decrease in distortion is small up to $M/M_0 \sim 2y$, which suggests that the magnetic clusters develop by the aggregation of Mn pairs (electron-hole sites), which we call dimerons. The location of such aggregated dimerons is constrained by the quenched disorder of the Ca distribution, which leads to filamentary magnetic clusters for $M/M_0 < 2y$. Increased local distortions should be found at higher temperatures when the dimerons dissociate.

The work at UCSC was supported in part by NSF Grant No. DMR0301971. We thank A. Millis and P. Littlewood for helpful discussions. The experiments were performed at SSRL, operated by the DOE, Division of Chemical Sciences, and by the NIH, Biomedical Resource Technology Program, Division of Research Resources. The magnet facility was supported by DOE Contracts No. DE-FG03-99ER-45773 and No. DE-AC03-76SF00515 and NSF Grants No. DMR-9985067 and No. DMR-9802737.

[1] C. H. Booth, F. Bridges, G. J. Snyder, and T. H. Geballe, Phys. Rev. B **54**, R15 606 (1996); T. A. Tyson *et al.*, Phys. Rev. B **53**, 13 985 (1996); G. Subías, J. García, M. G. Proietti, and J. Blasco, Phys. Rev. B **56**, 8183 (1997); C. H. Booth *et al.*, Phys. Rev. Lett. **80**, 853 (1998).
[2] C. H. Booth *et al.*, Phys. Rev. B **57**, 10 440 (1998).
[3] A. Lanzara *et al.*, Phys. Rev. Lett. **81**, 878 (1998).
[4] D. Cao, F. Bridges, D. C. Worledge, C. H. Booth, and T. Geballe, Phys. Rev. B **61**, 11 373 (2000).
[5] S. J. L. Billinge *et al.*, Phys. Rev. Lett. **77**, 715 (1996); D. Louca *et al.*, Phys. Rev. B **56**, R8475 (1997); D. Louca, T. Egami, and G. H. Kwei, J. Supercond. **12**, 291 (1999).
[6] D. Cao, F. Bridges, C. H. Booth, and J. J. Neumeier, Phys. Rev. B **62**, 8954 (2000); C. Meneghini *et al.*, J. Phys. Condens. Matter **14**, 1967 (2002).
[7] E. Dagotto *et al.*, Phys. Rev. B **58**, 6414 (1998); A. Moreo, S. Yunoki, and E. Dagotto, Science **283**, 2034 (1999); A. R. Bishop, T. Lookman, A. Saxena, and S. R. Shenoy, Europhys. Lett. **63**, 289 (2003); A. Weisse, J. Loos, and H. Fehske, Phys. Rev. B **68**, 024402 (2003); Y. Motome, N. Furukawa, and N. Nagaosa, Phys. Rev. Lett. **91**, 167204 (2003); J. Burgy, A. Moreo, and E. Dagatto, Phys. Rev. Lett. **92**, 097202 (2004).
[8] S. K. Sarker, J. Phys. Condens. Matter **8**, L515 (1996).
[9] T. V. Ramakrishnan, H. R. Krishnamurthy, S. R. Hassan, and G. V. Pai, Phys. Rev. Lett. **92**, 157203 (2004).
[10] P. S. Kumar, P. A. Joy, and S. K. Date, J. Phys. Condens. Matter **10**, L269 (1998).
[11] J. Lynn (private communication); C. S. Nelson *et al.*, Phys. Rev. B **64**, 174405 (2001).
[12] L. Downward, F. Bridges, D. Cao, J. J. Neumeier, and L. Zhou, Int. J. Mod. Phys. A **17**, 3726 (2003).
[13] G. G. Li, F. Bridges, and C. H. Booth, Phys. Rev. B **52**, 6332 (1995).
[14] EXAFS data analysis package—http://lise.lbl.gov.
[15] S. I. Zabinsky, J. J. Rehr, A. Ankudinov, R. C. Albers, and M. J. Eller, Phys. Rev. B **52**, 2995 (1995).
[16] Modeling with two Mn-O peaks (Ref. [3]) requires two amplitudes and two coupled σ's, thus, a single parameter is not available for comparison to the magnetization.
[17] $La_{0.79}Ca_{0.21}MnO_3$ may deviate since it is close to the metal-insulator boundary. See, Rivadulla *et al.*, Phys. Rev. B **70**, 172410 (2004). This sample also has a static distortion at low T, and is only 95% magnetized.
[18] P. V. Patanjali *et al.*, Phys. Rev. B **60**, 9268 (1999).
[19] At this point, the electrons in the magnetic cluster are delocalized, but we keep pairs of (undistorted) open and gray circles for counting purposes.